Chalcogenide Letters Vol. 20, No. 2, February 2023, p. 85 - 90

Structural, optical, and photocatalytic activity of ZnS:Er nanoparticles

B. Poornaprakash[a1], P. T. Puneetha [b1], M. S. P. Reddy[c], Y. L. Kim[a*]
[a]*Department of Electronic Engineering, Gangneung-Wonju National Univeristy, Gangneung, 25457, South Korea*
[b]*Department of Robotics and Intelligent Machine Engineering/College of Mechanical and IT Engineering, Yeungnam University, Gyeongsan 38541, South Korea*
[c]*Advanced Material Research Center, Kumoh National Institute of Technology, Gumi-39177, South Korea*

ZnS and Er (2 at%) doped ZnS nanoparticles (NPs) were synthesized through co-precipitation process. EDAX analysis confirmed that the presence of Er (III) ions in the prepared sample with an anticipated stoichiometry. TEM analyses displayed that the prepared NPs showed near spheroid shapes with an average size ranging from 4.8 to 5.2 nm. XRD measurements confirmed the authentic incorporation of Er (III) ions in the ZnS lattice. DRS measurements certified that Er (III) doping declines the ZnS bandgap from 3.72 to 3.56 eV. Magnetic measurements revealed that the Er-doped ZnS NPs displayed soft ferromagnetism and became better at higher doping concentrations. The Er (2 at%) doped ZnS NPs exhibited a higher rhodamine B dye degradation rate than the ZnS. Hence, the Er doped ZnS NPs are promising materials for dye degradation and optoelectronics.

(Received October 22, 2022; Accepted January 17, 2023)

Keywords: Zinc sulfide, Nanoparticles, Dye degradation

1. Introduction

The lack of access to safe drinking water is commonly related to poverty. Particularly, textile industries are one of the largest consumptions of water and complex chemicals during textile dispensation at the various processing stages and causes serious hurdles to the environment. The delivery of waste dyes is harmful to aquatic life as well as microorganisms [1]. Organic dyes are the most dangerous pollutants in wastewater delivery from textile industrial processes and cause environmental danger [2]. Amid the various biological and physical techniques available for the wastewater treatment including, reverse osmosis, air stripping, adsorption, ultra-filtration, and flocculation can be utilized for color removal of textile pollutants [3–5]. Zinc chalcogenide nanostructures conciliated photocatalysis is a proven photocatalyst, which can be possibly exploited for the annihilation of toxic compounds into safe compounds [6–8]. Zinc sulfide is exploited as the most capable photocatalyst for wastewater treatment [9, 10]. ZnS absorbs the light beneath the ultraviolet region, however its absorbance ability can be further amended through doping various rare earth /transition metal ions. Acting as an electron and/or hole trap is the vital function of these dopants. The trapping of charge carriers declines the recombination rate of electron–hole pairs and consequently, enhances the lifetime of charge carriers emerging in an improvement in photocatalytic activity [11]. In the present work, ZnS and Er (2 at%) doped ZnS NPs have been fabricated via co-precipitation process and studied their morphology, structural, optical and dye degradation properties.

* Corresponding author: ylkim@gwnu.ac.kr
[1]First and second authors are equally contributed.
https://doi.org/10.15251/CL.2023.202.85

2. Experimental and characterization

ZnS and Er (2 at%) doped ZnS NPs were synthesized using co-precipitation route. For ZnS sample, 0.05 M of zinc nitrate (0.0548 (pristine) was dissolved in 50 mL of deionized water and stirred for 20 min. An aqueous solution (0.05 M) of Na_2S (0.195 g) was added to the above zinc solution and stirred for 6 h at 60 °C. The samples were filtered and cleansed with polar solvents, followed through heated at 70 °C for 15 h. For Er doped ZnS sample, 0.05 M of zinc nitrate (0.0426 g) and required amount of erbium nitrate (0.044 g) were dissolved in to 5o mL of deionized water and stirred for 20 min. The remaining process was the same pristine ZnS.

The employed characterizations including, Energy-dispersive X-ray spectroscopy (EDAX), X-ray diffraction (XRD), low-resolution transmission electron microscopy (TEM), and diffuse reflectance spectroscopy (DRS)) are the alike used in our published article [12]. The photodegradation of rhodamine-B process and utilized tools of the above samples are alike our recent published article [12].

3. Results and discussions

Fig. 1 illustrates the EDAX spectra of (a) ZnS and (b) Er (2 at.%) doped ZnS NPs. The compositional analysis depicts the presence of Er, S and Zn signals in the Er doped ZnS sample, designating that the samples are made up of erbium , sulfur, and zinc. Only zinc and sulfur signals have been noticed in the ZnS samples. These results confirm the high purity of the prepared NPs. The morphology and size of the ZnS and Er (2 at%) doped ZnS NPs were analyzed through TEM, as depicted in Fig. 2 (a) and (b). All the samples consist of trivial agglomeration and spherical shaped. The inset of Fig. 2 (a and b) shows the particles size distribution of the prepared samples. The average sizes of the prepared NPs assessed with the and are 5.2 and 4.8 nm for ZnS and Er (2 at%) doped ZnS NPs.

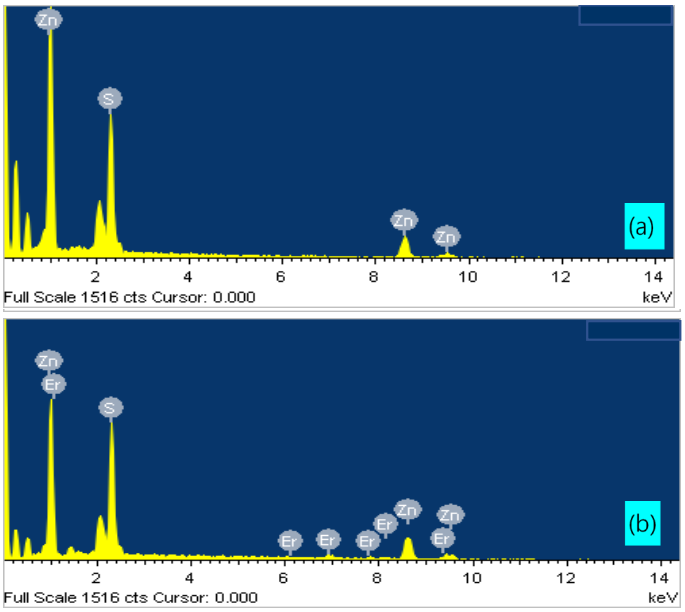

Fig. 1. EDAX spectra of (a) ZnS and (b) Er (2 at%) doped ZnS NPs.

It could be due to the 4f-4f transition of Er (III) ions from the ground state ($^4I_{15/2}$) to different excited states [13]. In addition, the absorption edge of the ZnS NPs displayed a red shift after Er doping, designating decline in bandgap. The bandgap of the fabricated NPs was calculated from the reflectance spectra through using Kubelka-Munk plots (Fig. 2 (c)) and are 3.76 and 3.56 eV for ZnS and er (2 at%) doped ZnS NPs. As is well known, the redshift of energy gap in band

gap is interpreted as attributed to the spin-exchange interactions between sp band and localized spins of the Er dopant [12, 14].

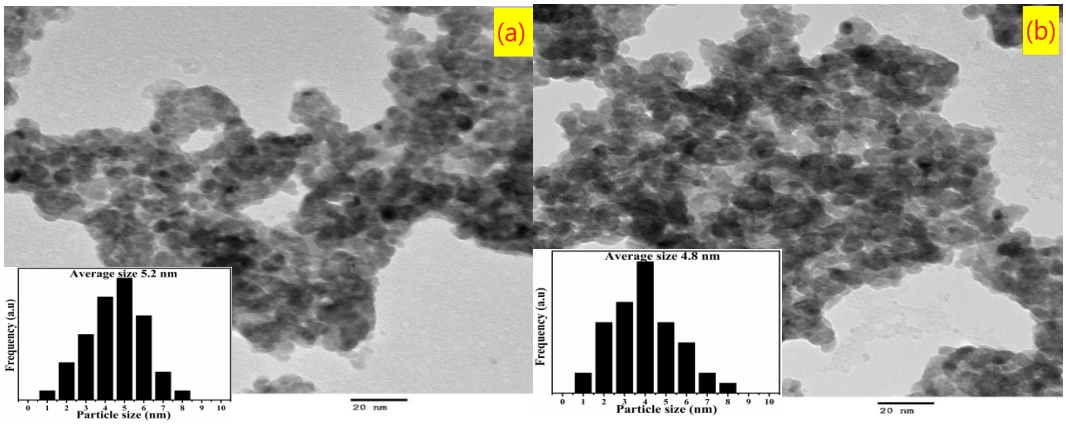

Fig. 2. TEM images of (a) ZnS and (b) Er (2 at%) doped ZnS NPs.

The X-ray diffraction patterns of the ZnS and Er (2 at%) doped ZnS NPs are illustrated in Fig. 3 (a) ; the identical peaks, belonging to the (111), (220), and (311) reflections, are in well agreement with the cubic ZnS phase. Additionally, no foreign peaks were identified, which proposing that the Eu (III)t ions are successfully dispersed inside the ZnS matrix. After Er doping, the peak positions of the ZnS displayed a slight shift to lower side and it may be attributed to the diverse ionic radius of the zinc (II) as well as erbium (III) ions. The average crystallite sizes evaluated according to Debey-Scherrer's equation [19], were found to be in the range of 4.2 to 4.8 nm. Fig. 3 (b) illustrates the DRS spectra of the pristine and Er (2 at%) doped ZnS NPs. The absorption bands at 378, 406, 442, 450, 487, 520, 652, and 795 nm indicate the existence of Er (III) ions in the ZnS NPs.

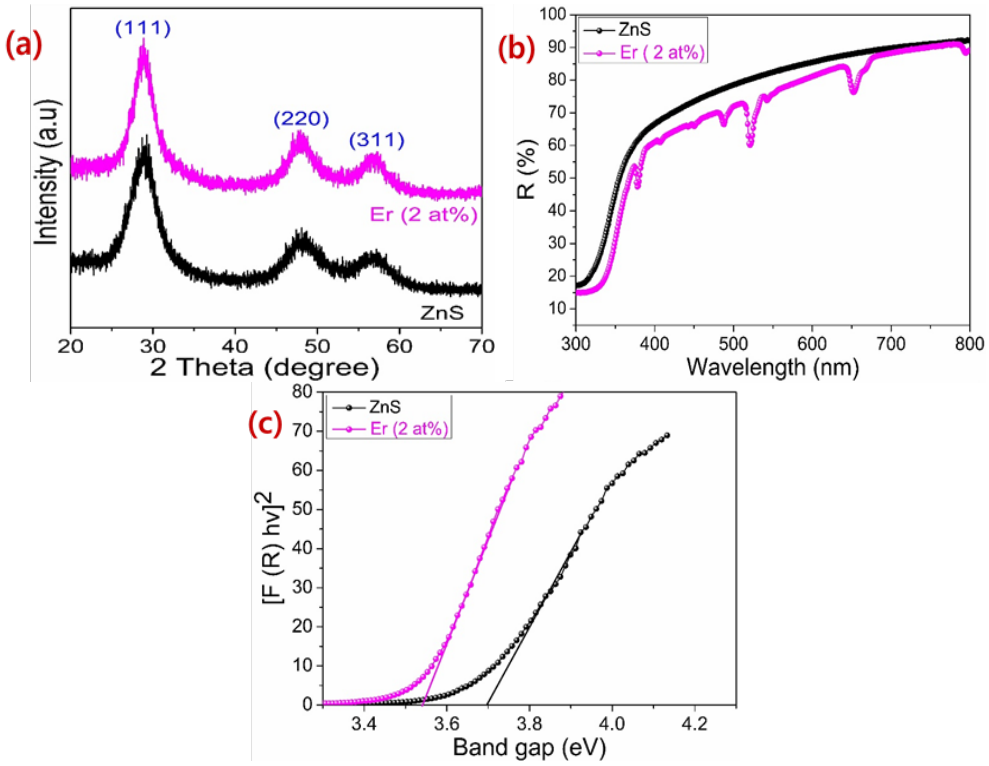

Fig. 3 (a) XRD, (b) DRS, and (c) Kubelka-Munk plots of ZnS and Er (2 at%) doped ZnS NPs.

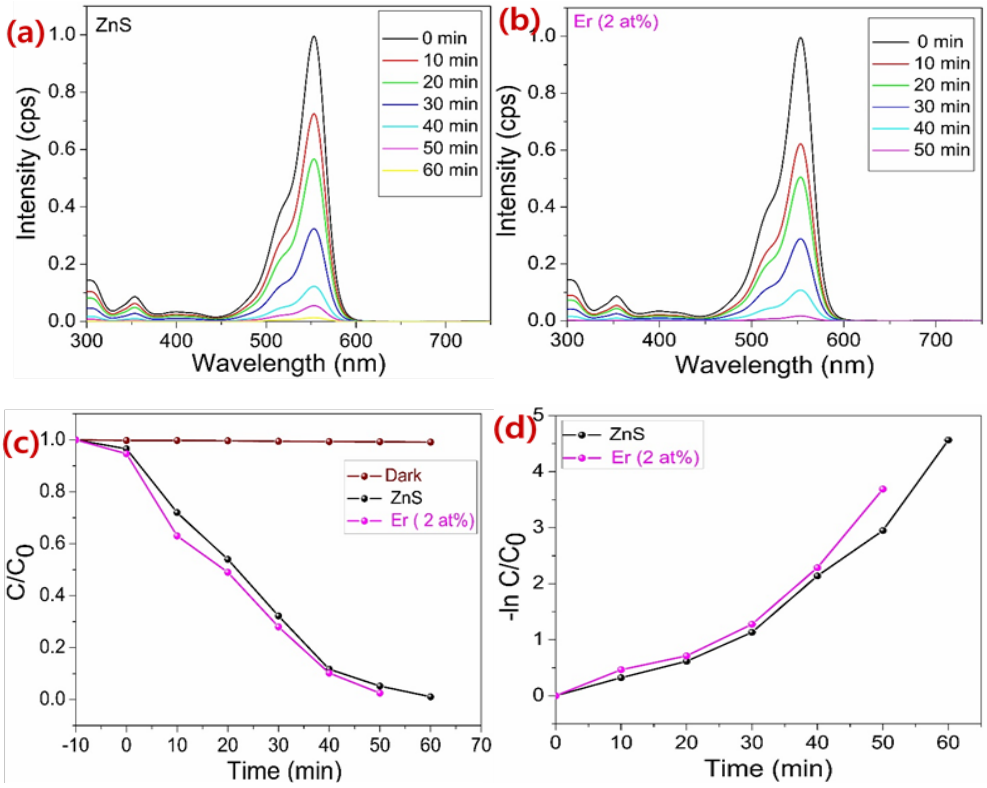

Fig. 4 (a & b) UV–vis absorption spectra changes (c) Photocatalytic activities, and (d) kinetic linear simulation curves of Rhodamine-B photocatalytic degradation of ZnS and ZnS:Tb (2 at%) nanoparticles.

Er (2 at%) doped ZnS NPs were found to have an enriched photocatalytic activity compared to that of the ZnS sample. ZnS and Er (2 at%) doped ZnS NPs were used as nanocatalysts for the degradation of RhB in solution, beneath simulated solar light. The significant reduction in the optical band gap of the Er (2 at%) doped ZnS NPs prompted us to investigate the degradation of the general RhB dye beneath light irradiation. Fig. 4 (a & b) displays the UV-Vis absorption spectra of RhB on the (a) ZnS and (b) Er (2 at%) doped ZnS NPs. The complete degradation of RhB in aqueous solution required 60 and 50 min for ZnS and Er (2 at%) doped ZnS NPs, respectively. For comparison, we employed the photodegradation of RhB in the dark and without a nanocatalyst. Only a trivial photodegradation of rhodamine B was observed in this blank test. A graph of C/C_0 vs. time revealed that the Er (2 at%) doped ZnS NPs was quicker than the bare NPs, as displayed in Fig 4 (c) . Fig. 4 (d) illustrates the kinetics of the RhB solution by the ZnS and Er (2 at%) doped ZnS samples under simulated solar light illumination. Based on these results, we presumed that the degradation of RhB under the simulated sun light irradiation in the presence of ZnS:Er NPs was influenced by several parameters such as concentration of doping impurities, crystallite size, optical bandgap, creation of defect sites, and trapping locations. In the present report, grain size as well as energy gap of the synthesized NPs was decreased with respect to Er ion doping concentrations and these observations were noticed in structural and optical studies. Meanwhile, substitution of Er at Zn site creates the defect sites and are acted as trapping locations. In this perception, when the electrons are transition from V.B. to C.B. under photons induction, holes are created in V.B. and electrons are generated in C.B. Fig. 5 presents the proposed photocatalytic mechanism for the decolorization of RhB beneath simulated solar light irradiation, with the reaction steps illustrated in Eqs. (1)–(7). Following the electron transfer from the V.B. to the C.B. of ZnS under simulated solar light illumination (Eq. (2)), the accumulated electrons can be rapidly trapped through the defect sites created by interstitial occupation of erbium ions (Eq. (3)) at zinc sites and consequently hindering the recombination of holes with

electrons. These electrons are then scavenged through molecular oxygen to generate the superoxide radical anion $O_2^{\cdot-}$ (Eq. (4)), followed by the formation of H_2O_2 (Eq. (5)). The radicals may react to generate the hydroxyl radical $OH^{\cdot}$. The photoinduced holes formed in the valence band react with the intermediate hydroxyl groups as well as water molecules to generate hydroxyl radicals, as shown in Eq. (6). Eventually, pollutant molecules are oxidized through these oxidants as well as subsequently mineralized into the eventual outcomes (Eq. 7). These interesting results confirm that Er doping is a reliable approach for increasing the photocatalytic activity of ZnS sample. Yanhua et al. [15] observed improved photocatalytic performance in ZnS urchin-like nanostructures via erbium doping. However, no literature on the photocatalytic activity of Er doped ZnS NPs is available for comparison with our results.

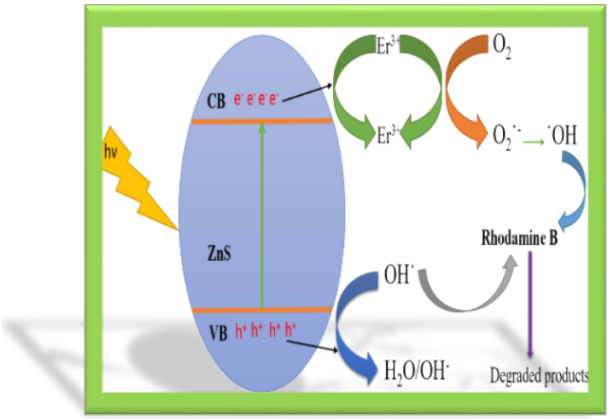

Fig. 5. Schematic of a plausible mechanism for photocatalytic degradation.

4. Conclusions

In summary, ZnS and Er (2 at%) doped ZnS NPs were synthesized via co-precipitation process. The structural, optical, and photocatalytic degradation properties were assessed. The XRD investigation asserted the successful inclusion of Er (III) in the parent matrix. Morphology analysis revealed that the fabricated samples trivially polydisperse, with average size ranging from 4.8 to 5.2 nm. A reduction in the optical bandgap was achieved in the ZnS NPs after Er doping. Eu (2 at%) doped ZnS NPs displayed robust photocatalytic efficiency, attaining 98% degradation and was higher than those of ZnS. Hence the Er doped ZnS NPs may find applications in the field of photocatalysis and optoelectronics.

Acknowledgments

This work was supported by the National Research Foundation Korea funded by the Ministry of Science, ICT and Fusion Research (Grant No: 20201G1A1014959). This work was supported by the Technology development Program (S3038568) funded by the Ministry of SMEs and Startups (MSS, Korea). The study was supported by the National Research Foundation of Korea (NRF) funded by the Ministry of Science (Grant Nos. 2022R1I1A1A01064248).

References

[1] Pritam Borker, A.V. Salker, Mater. Sci. Eng., B 133 (2006) 55-60; https://doi.org/10.1016/j.mseb.2006.05.007

[2] Michael R. Hoffmann, Scot T. Martin, Wonyong Choi, Detlef W. Bahnemann, Chem. Rev. 95

(1995) 69-96; https://doi.org/10.1021/cr00033a004

[3] Tim Robinson, Geoff McMullan, Roger Marchant, Poonam Nigam, Bio. Resour. Technol. 77 (2001) 247-255; https://doi.org/10.1016/S0960-8524(00)00080-8

[4] Ajay Singh, Karakoti, Ritesh Shukla, Rishi Shanker, Sanjay Singh, Adv. Colloid. Interface Sci. 215 (2015) 28-45; https://doi.org/10.1016/j.cis.2014.11.004

[5] Christina Marie Tyrakowski, Preston Todd Snee, Phys. Chem. Chem. Phys. 16 (2014) 837-855; https://doi.org/10.1039/C3CP53502A

[6] Udaya Aruldoss, L. John Kennedy, J. Judith Vijaya, G. Sekaran, J. Colloid Interface Sci. 355 (2011) 204-209; https://doi.org/10.1016/j.jcis.2010.11.073

[7] N. Clament Sagaya Selvam, J. Judith Vijaya, L. John Kennedy, J. Ind. Eng. Chem. 51 (2012) 16333-16345; https://doi.org/10.1021/ie3016945

[8] N. Clament Sagaya Selvam, A. Manikandan, L. John Kennedy, J. Judith Vijaya, J. Colloid Interface Sci. 389 (2013) 91-98; https://doi.org/10.1016/j.jcis.2012.09.014

[9] Hengbo Yin, Yuji Wada, Takayuki Kitamura, Shozo Yanagida, Environ. Sci. Technol. 35 (2011) 227-231; https://doi.org/10.1021/es001114d

[10] Qingrui Zhao, Yi Xie, Zhigao Zhang, Xue Bai, Cryst. Growth Des. 7 (2007) 153-158; https://doi.org/10.1021/cg060521j

[11] Ruby Chauhan, Ashavani Kumar, Ram Pal Chaudhar, J. Sol-Gel Sci. Technol. 67 (2013) 376-383; https://doi.org/10.1007/s10971-013-3091-9

[12] B. Poornaprakash, Herie Park, K. Subramanyam, S.V. Prabhakar Vattikuti, Kamakshaiah Charyulu Devarayapalli, Seung Hyun Nam, Y.L. Kim, M. Siva Pratap Reddy, Myung Gwan Hahm, Vasudeva Reddy Minnam Reddy, Ceram. Int. 47 (18) (2021) 26438-26446; https://doi.org/10.1016/j.ceramint.2021.06.055

[13] M.S. Sajna, Sunil Thomas, K.A. AnnMary, Cyriac Joseph, P.R. Biju, N.V. Unnikrishnan, J. Lumin. 159 (2015) 55-65; https://doi.org/10.1016/j.jlumin.2014.10.062

[14] A. Bouaine, R.J. Green, S. Colis, P. Bazylewski, G.S. Chang, A. Moewes, E.Z. Kurmaev, A. Dinia, J. Phys. Chem. C, 115 (2011) 1556-1560; https://doi.org/10.1021/jp1088096

[15] Yanhua Tong, Feng Cao, Jintian Yang, Minhong Xu, Chu Zheng, Xingyu Zhu, Di Chen, Min Zhang, Fan Huang, Jie Zhou, Lixiao Wang, Mater. Chem. Phys. 151 (2015) 357-363; https://doi.org/10.1016/j.matchemphys.2014.12.005